Journal of Marine Research, 59, 795–812, 2001

Phytoplankton seasonal distribution from SeaWiFS data in the Agulhas Current system

by E. Machu[1,2] and V. Garçon[1]

ABSTRACT

The interocean conduit for warm Indian Ocean water into the Atlantic Ocean is the Agulhas system which plays an important role in maintaining the global thermohaline circulation. The frontal system formed by the Agulhas Return Current (ARC) and the Subtropical Convergence (STC) is also a region of intense mesoscale activity presenting enhanced levels of biological production and chlorophyll *a*.

We jointly analyzed three different satellite data sets to relate the remotely sensed distribution of phytoplankton (SeaWiFS ocean color data) to the dynamical environment (Topex/Poséidon-ERS sea level anomalies -SLA- and sea-surface temperature -SST-) to gain insight into the seasonal behavior of the Agulhas Current system. We used a wavelet analysis to retrieve the characteristic wavelengths of the ARC and STC associated to their meandering. By meridionally averaging (between 15–45E) the two-dimensional power Hovmöller of each signal (Chl *a,* SLA, and SST), we obtained a seasonal average variance for Chl *a,* SLA and SST as a function of latitude.

Within the double frontal Agulhas and Subtropical frontal system, an extended temporal maximum in chlorophyll *a* concentration is observed in spring-summer-fall and a well-marked minimum occurs in winter, in phase opposition with the southwest Indian Ocean subtropical gyre north of the frontal system. Seasonal changes in strength of cross-frontal mixing with the subtropical gyre, in density strength of the juxtaposed fronts, and in mixed-layer depth and light availability seem the most likely explanations for the observed spatial and seasonal variability of the chlorophyll *a* distribution.

1. Introduction

The Agulhas Current system (Fig. 1) is thought to be a key link in the maintenance of the global overturning circulation. In the upper ocean this link is the intermittent intrusion into the southeast Atlantic Ocean of warm and salty waters spawned from the retroflection (R) of the Agulhas Current (AC) (Fig. 1). These waters contribute to the warm water route which counter-balances the leakage of North Atlantic Deep Waters from the Atlantic basin (Gordon, 1986; Gordon *et al.,* 1992). The Agulhas system consists of three parts: a source region, the Agulhas Current (AC) proper and a system of outflows (Fig. 1). All have a

1. LEGOS/UMR5566, CNRS, 18 Avenue Edouard Belin, 31401 Toulouse Cedex 4, France. ***email: veronique.garcon@cnes.fr.***

2. Present address: CERFACS, 42 Avenue Gaspard Coriolis, 31057 Toulouse Cedex 1, France.

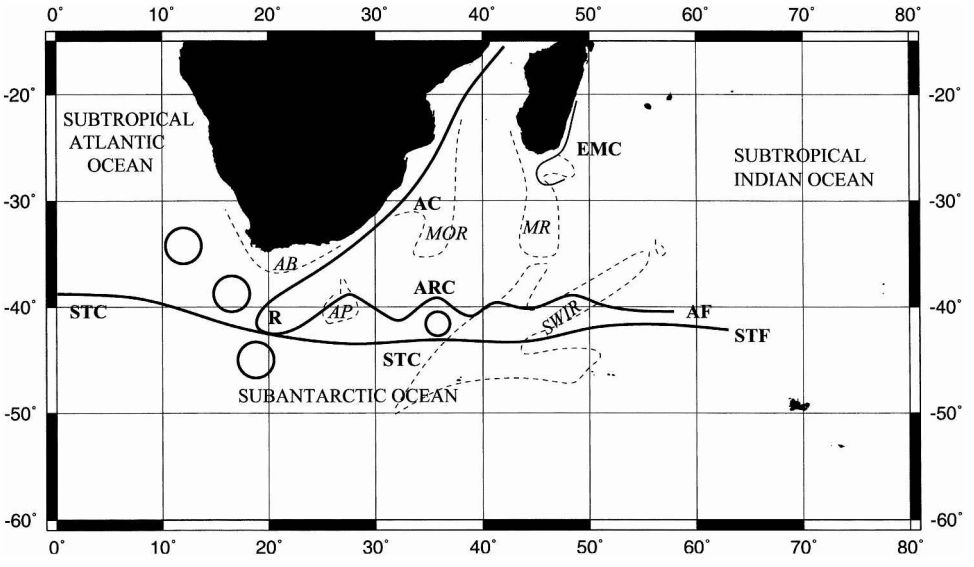

Figure 1. Scheme of the upper circulation in the Agulhas region. Source region: EMC: East Madagascar Current. Agulhas Current proper: AC: Agulhas Current. Outflows system: R: Retroflection; AF: Agulhas Front; ARC: Agulhas Return Current; STC: Subtropical Convergence; STF: Subtropical Front. Topographic features: AB: Agulhas Bank; AP: Agulhas Plateau; MR: Madagascar Ridge; MOR: Mozambique Ridge; SWIR: Southwest Indian Ridge.

decisive influence on the manner in which the AC fulfills its task as a link in the global thermohaline cell.

The source region includes three areas: a flow from the Mozambique channel carrying Indian Tropical Surface Water (TSW), a flow from the southeast of Madagascar via eddies spawned to a large extent from the East-Madagascar current retroflection (Lutjeharms, 1988; Lutjeharms and Machu, 2000) and a recirculation cell in the southwest Indian Ocean subgyre south of Madagascar that extends eastward to about 70E (Stramma and Lutjeharms, 1997). These various tributaries form the AC proper which intensifies along its southwestward route. The AC intensification between 32S and the retroflection could result from a recirculation cell centered at 30E, 38S seen in 3 years of Geosat altimetric data by Feron *et al.* (1998).

The retroflection, the rings, and the Agulhas Return Current (ARC) flowing eastward along the subtropical convergence (STC), constitute the outflows subsystem of the Agulhas system. The hydrodynamics of the fronts associated with the ARC, the Agulhas Front (hereafter AF) and to the STC, the subtropical front (STF), have been widely studied (Lutjeharms and Valentine, 1984; Belkin and Gordon, 1996; and Holliday and Read, 1998) (Table 1). To determine the zonal position of the fronts, Lutjeharms and Valentine (1984) used the SST gradient. The more recent hydrographic cruises crossing these fronts collected surface and subsurface temperature and salinity observations in order to deter-

Table 1. Latitudinal location of the Agulhas and subtropical fronts reported in three different studies. The locations and surface ranges of the temperature and salinity result from a compilation of hydrographic sections (std dev. is for standard deviation.)

	Agulhas Front (AF)		
	Latitude (°S)	SST (°C)	S (psu)
Holliday & Read (1998)	38.0–41.2	20.7–17.2	35.70–35.22
Belkin & Gordon (1996)	38–40	21.7–18.7	35.54–35.39
Lutjeharms & Valentine (1984)	39.2–40.0 std dev. 1.3–1.3	21.0–15.7	
	Subtropical Front (STF)		
	Latitude (°S)	SST (°C)	S (psu)
Holliday & Read (1998)	41.1–43.0	17.0–10.6	35.35–34.05
Belkin & Gordon (1996)	42–43	15.1–10.3	35.18–34.30
Lutjeharms & Valentine (1984)	40.6–42.6 std dev. 1.4–1.5	17.9–10.6	

mine more accurately their position. Holliday and Read (1998), from continuously sampled thermosalinograph data along WOCE sections, found the AF always separated from the STF whereas previous studies (Lutjeharms and Valentine, 1984; Belkin and Gordon, 1996) often observed them merged. The observed location of the fronts depends on longitude, season of the section, and the angle at which vessels crossed the front. From these different estimations (Table 1), the AF is localized between 38S and 41.2S and the STF between 40.6S and 43S (Lutjeharms and Valentine, 1984; Holliday and Read, 1998; Cruise DI201) in our region of interest (from the retroflection-15E to the Madagascar Ridge-45E).

There have been many efforts to estimate and seasonality of the Agulhas system based on either altimetry data (sea-surface height) (Quartly and Srokosz, 1993; Matano *et al.,* 1998), numerical modeling studies (Lutjeharms and van Ballegooyen, 1984; De Ruijter and Boudra, 1985; Ou and De Ruijter, 1986; Matano *et al.,* 1998, 1999; Biastoch *et al.,* 1999) or *in situ* hydrographic data (Pearce and Gründlingh, 1982; Ffield *et al.,* 1997). These efforts have produced contradictory pictures, some showing a marked seasonality, others no significant seasonal variation of the system.

The frontal system of the AF and STF is one of the most energetic regions in the world ocean (Ducet *et al.,* 2000). Mesoscale features such as meanders, eddies, filaments and fronts have an influence on oceanic primary productivity and plankton distribution (Flierl and Davis, 1993; Oschlies and Garçon, 1998; McGillicuddy *et al.,* 1998; Spall and Richards, 2000). Consequently, mesoscale variability is a pervasive feature of satellite ocean color.

In the present study, we propose to relate the remotely sensed phytoplankton distribution to the physical environment as observed by altimetry and infrared radiometry with the

objective to help resolve differences between prior efforts to estimate the seasonality of the Agulhas system. Applying a wavelet analysis to three different satellite data sets (ocean color, altimetric and sea-surface temperature data), we retrieve the characteristic wavelengths of the AF and STF in order to study their possible seasonal zonal movements. Dynamical scenarios to explain the spatial and seasonal variability of the phytoplankton distribution are given following the interpretation of results.

2. Data

Mapped Sea Level Anomaly (MSLA) used in this study were obtained from the combined processing of the Topex/Poséidon (T/P) and ERS-2 data. Maps were produced every 10 days from data covering a 20-day period with a resolution of 0.25 degree by 0.25 degree. Sea Level Anomalies (SLA) are relative to a 3-year average (January 1993 to January 1996). Maps were obtained using an improved space/time objective analysis method which takes into account long wavelength errors correlated noise (Le Traon *et al.,* 1998).

Sea-surface temperature (SST) is processed by the Naval Oceanographic Office. The SST retrieval-generation is described in May *et al.* (1998). With regard to the daily product used, the 1/10 degree gridded K10 composite is updated with the latest SST retrievals (currently only using satellite retrievals from NOAA-14). After all grid cells containing new data are updated, a single smoothing step takes place that updates the grid with an average of the grid cell and all surrounding grid cells.

Phytoplankton pigment concentrations were obtained from the SeaWiFS (Sea-viewing Wide Field-of-View Sensor) products (level 3 binned data, monthly, version 2) generated by the NASA Goddard Space Flight Center (GSFC) Distributed Active Archive Center (DAAC) (McClain *et al.,* 1998). The bins correspond to grid cells on a global grid, with each cell approximately 9 by 9 km.

Altimetry provides dynamic heights (an integrated measure), the ocean color sensor observes the first few meters (depending on the turbidity of the water) and the radiometer gives the temperature of the first micrometers of the water column. We expect to take advantage of the different information contained in these different data sets to study the physical-biological interactions.

3. Methodology

The wavelength and amplitude of the Rossby wave associated with the ARC have been determined by a wavelet analysis in a previous study in jointly analyzing the signals of phytoplankton pigment concentrations (SeaWiFS) and SLA (T/P-ERS2) (Machu *et al.,* 1999). Two distinct dynamical scenarios of the Agulhas system (weekly SeaWiFS images of October 1997 and January 1998) yield different dominant wavelengths for the ARC Rossby wave simultaneously retrieved from the chlorophyll *a* and SLA signals (Machu *et al.,* 1999). Here, we propose to retrieve the characteristic wavelengths of the AF and STF

in order to study their possible zonal seasonal movements. We thus analyzed the first year of SeaWiFS monthly images (October 1997–September 1998), simultaneously with monthly T/P-ERS2 and SST data by applying an extension of the wavelet analysis, the power Hovmöller. This is the first time simultaneity of altimetric data, ocean color and SST data is achieved providing a unique opportunity to analyze the large-scale distribution of phytoplankton biomass in relation to forcing caused by the physical environment.

The wavelet analysis can be summarized as follows. Let x_n denote a signal that varies with equal spacing δx along an x-axis and $n = 0, \ldots, N - 1$. The x-axis will follow a latitude circle. Also assume that one has a wavelet function, $\psi_0(\eta)$ (mother wavelet) that depends on a nondimensional distance parameter η. To be admissible as a wavelet, this function must have zero mean, have a Fourier transform that exists, and be localized in both distance and frequency space (Farge, 1992). The continuous wavelet transform of a discrete sequence x_n is defined as the convolution of x_n with a scaled and translated version of $\psi_0(\eta)$:

$$W_n(s) = \sum_{n'=0}^{N-1} x_{n'} \psi^* \left[\frac{(n' - n)\delta x}{s} \right],$$

where the (*) indicates the complex conjugate. By varying the wavelet scale s and translating along the localized distance index n, one can construct a picture showing both the amplitude of any features versus the scale and how this amplitude varies with distance.

Widely used in geophysics, the Morlet wavelet is the mother wavelet chosen here (as in Machu *et al.,* 1999). Since the Morlet wavelet is complex, the wavelet transform is also complex. One defines the local wavelet power spectrum as the square of the modulus of the wavelet coefficients $|W_n(s)|$ (Torrence and Compo, 1998). It is usually normalized to have unit energy.

We perform our analysis between 15 and 45E and we scan the latitude circles from 36 to 45S. The extraction of the wavelet coefficient maxima from the local wavelet power spectrum gives us the range of the wavelength associated to the meanders of the ARC and STC, found here equal to 380–760 km (not shown). To examine fluctuations in power over this range of scales, one can define the scale-averaged wavelet power as the weighted sum of the wavelet power spectrum over scales 380 km to 760 km, and hence, one can assess the spatial variability of a field of data. At each latitude, the wavelet power spectrum is computed using the Morlet wavelet, and the scale-averaged wavelet power over the 380–760 km band is calculated from the equation:

$$\overline{W}_n^2 = \frac{\delta j \delta x}{C_\delta} \sum_{j=j_1}^{j_2} \frac{|W_n(s_j)|^2}{s_j}$$

where δj is the spacing between discrete scales and the factor C_δ comes from the reconstruction of a δ-function from its wavelet transform using the function $\psi_0(\eta)$. This way we obtain a two-dimensional longitude-latitude diagram power Hovmöller. The

meridional average of the power Hovmöller then gives a measure of the global 380–760 km wavelength variance in the selected longitude band (15E–45E) for each signal (SLA, chlorophyll *a* and SST).

4. Results

Figure 2 clearly illustrates seasonal variability in the Agulhas system. In austral summer (February, Fig. 2a), the meandering of the ARC, associated to a topographic Rossby wave (Weeks and Shillington, 1994), is well defined delimiting high chlorophyll *a* concentrations to the south from the northern part characterized by low pigment levels (0.1 mgChl*a*/m^3). In contrast, the monthly August scene (Fig. 2b, austral winter conditions) presents a diffuse AF, lower concentrations in the frontal system and an enriched background level of chlorophyll *a* in the southwest Indian Ocean. We averaged chlorophyll *a* concentrations for each season within the box 25E–45E; 25S–35S (Table 2) for two years (October 1997–September 1999). A seasonal behavior arises from these mean concentrations with maxima (minima) in austral winter (summer) reflecting the two different scenarios shown in Figure 2.

Figure 3 shows the average variance as a function of latitude resulting from a meridional average (between 15–45E) of the two-dimensional (latitude–longitude) power Hovmöller described in the previous section. The variances are normalized by the maximum variance achieved over one year (October 1997–September 1998) and between 36S and 45S for the three types of data (SLA, SST and ocean color). The high variance levels correspond to high amplitude of the signal (SLA, chlorophyll *a* or SST) and/or a well defined wave associated to the meanders of the AF and STF since we averaged the wavelet coefficients over the band of wavelengths corresponding to the wavelet coefficient maxima.

The full line shows the variability of the SLA signal. A broad region of high variance emerges between 37.5S and 40.5S and is likely to represent the variability of the ARC region (Fig. 3). The local maximum at 42S, in summer, would indicate the STF. Although the STF is a wider front, the transport associated with it is weaker than that associated with the AF (Read and Pollard, 1993). On the map of SLA on February 13th, 1998, we superimposed the 21°C, 17°C and 13°C isotherms (Fig. 4) which represent the upper and lower temperature limits of the AF and the middle temperature of the STF (Table 1), respectively, for summer conditions. The highest mesoscale variability present in the ARC region gives us some confidence in our interpretation; i.e., the higher average variance between 37.5 and 40.5S corresponds to the ARC (this pattern is observed on most summer SLA maps combined with the 21°C, 17°C and 13°C isotherms). Based on this front separation, winter and summer months present a higher average variance than fall and spring months in the STF (Fig. 3). AF average variance follows an opposite trend with higher values during spring and fall months (Fig. 3).

The SST average variance (dotted line) exhibits three main local maxima (mostly visible in winter and not present throughout the year) which we attribute to the AF (2 northern maxima) and STF (southern one) (Fig. 3). Cruises led across these fronts often show a

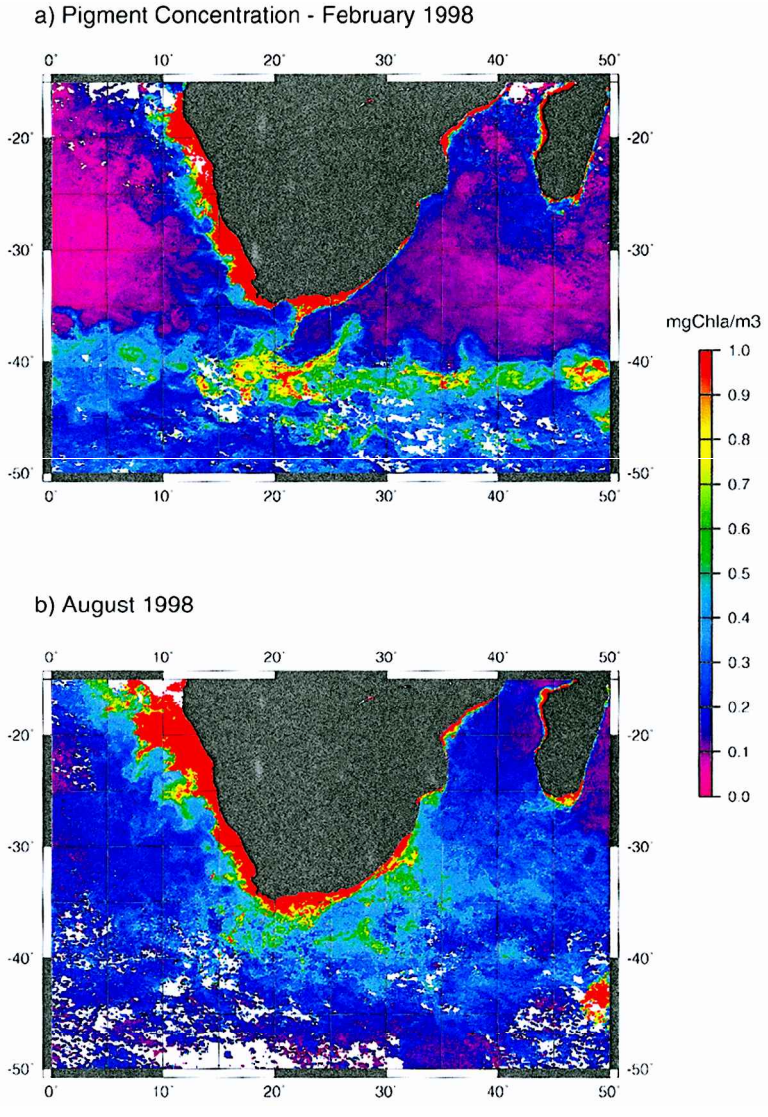

Figure 2. Surface pigment concentrations (mgChl*a*/m^3) from SeaWiFS monthly composites for (a) February, 1998 (mid-austral summer), (b) August, 1998 (mid-austral winter). Pixels with concentrations higher than 1 mgChl*a*/m^3 are red.

subsurface expression of the STF located predominantly north of the surface expressions (Lutjeharms and Valentine, 1984). The highest variance of SST is often situated southward of the subsurface signal deduced from the SLA (Fig. 3). In the STF, the SST variance presents the same trend as SLA with higher levels for summer and winter months as compared with spring and fall months (Fig. 3). Note that the winter STF peak (~41S) is

Table 2. SeaWiFS mean seasonal chlorophyll concentrations (mgChl*a*/m^3) in the southwest Indian Ocean: 25E–45E, 25S–35S). The number of grid points giving the monthly mean number of valuable pixels for each season varied between 14696 and 14845.

Date	Average chlorophyll concentration (mgChl*a*/m^3)
Spring 1997	0.22
Summer 1998	0.16
Fall 1998	0.25
Winter 1998	0.39
Spring 1998	0.23
Summer 1999	0.18
Fall 1999	0.23
Winter 1999	0.33

well pronounced. It could be due to the SST seasonality which is weaker within tropical waters than in Subantarctic waters. Thus a stronger gradient would result and be better detected. For a given season, the SST average variance of the AF differs from the SLA behavior (Fig. 3). Mapped SLA, as an alternate of troughs and crests, slightly offset in latitude (pink minima and red maxima in Fig. 4) produce two local maxima as we scan over latitude (Fig. 3). Mapped SST, presenting a wavelike signal, yields a smoother variance. SST average variance presents a maximum in fall months and a minimum in winter months (between 37.5 and 40.5S) (Fig. 3).

During spring and summer, a "biological subtropical front" with high levels of variance of chlorophyll *a* was present between the AF and STF (Fig. 3). The fall season shows the highest variance within the dynamical AF (38–40.5S) and the lowest variance levels occur in winter. Note that chlorophyll *a* north of the dynamical AF (37–38S) has low variances for the spring and summer months in comparison with fall and winter months (Fig. 3). As the dynamical AF does not show seasonal zonal movements and, keeping in mind Figure 2 (i.e. diffuse AF in term of chlorophyll *a*), increased variance levels in fall/winter may result from increased chlorophyll concentrations rather than from a more significant Rossby wave. For the STF, one can observe a steady decrease in chlorophyll variance from spring until winter. The area between the AF and STF fronts exhibits a chlorophyll *a* enrichment except during winter (Fig. 3).

Figure 5 shows the time-longitude diagram of two years of SeaWiFS chlorophyll *a* concentrations (October 1997–September 1999). All scales (including those smaller than 380 km and larger than 760 km) are present in these chlorophyll distributions. At 36S (Fig. 5a), a section between 15 and 60E crosses the Agulhas Current. A distinct annual cycle emerges from the time-longitude diagram of this section with minimal concentrations in summer and fall and maxima in winter and spring. At 38S (Fig. 5b), at the AF crossing, a shorter minimum occurs in summer. In the frontal system (41S, between the AF and STF, Fig. 5c), we observe an opposite phase signal with minimal (maximal) concentrations in winter (summer). The period of chlorophyll enrichment increases with higher concentrations. A semi-annual frequency seems to emerge and combines with the

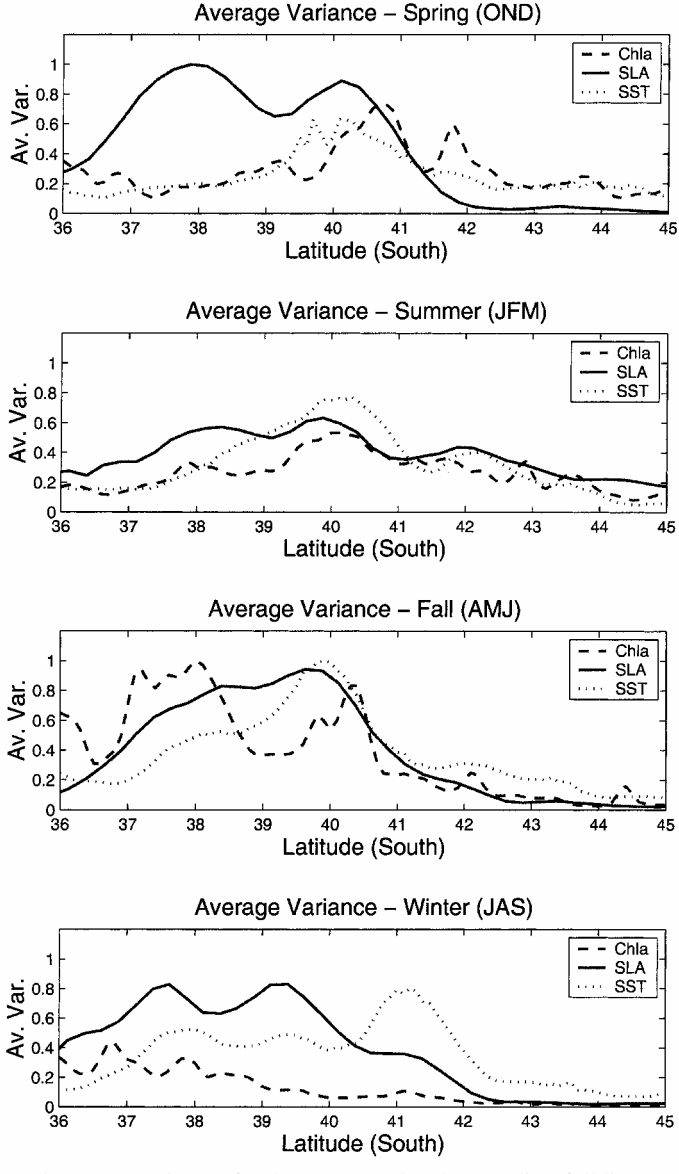

Figure 3. Seasonal average variances for the SLA (sea level anomalies, full line), SST (sea-surface temperature, dotted line) and ocean color (dashed line) data as a function of latitude resulting from a meridional average (between 15–45E) of the two-dimensional power Hovmöller. Variances are normalized by the maximum variance achieved for each signal over one year, October 1997–September 1998, and between 36 and 45S. The chlorophyll signal has been smoothed over three points (increment is 0.1°) with a Gaussian filter. ARC: Agulhas Return Current; STC: Subtropical Convergence. OND denote October, November, December, JFM January, February, March, AMJ April, May, June, and JAS July, August and September.

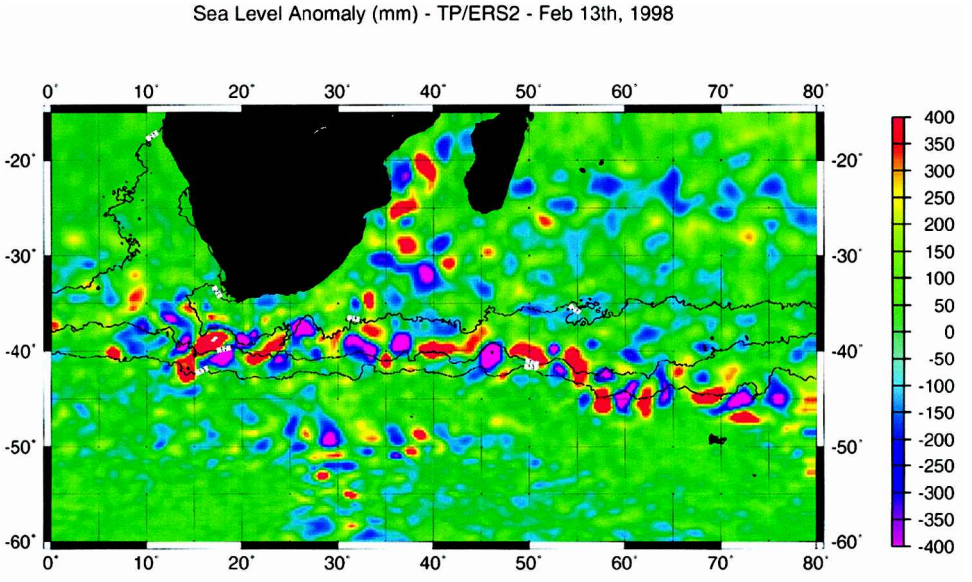

Figure 4. Mapped sea level anomalies (mm) from the combined T/P and ERS-2 altimeters. Black contours are the 21°C, 17°C and 13°C isotherms deduced from the SST data processed by the NAVOCEANO. These isotherms characterize the upper (northern) and lower (southern) temperature limits of the AF and the middle temperature of the STF, respectively, for summer conditions.

annual frequency to create an asymmetry in the total annual cycle. Southward (43–45S, data not shown), the chlorophyll distribution again exhibits a seasonal cycle with greater levels in summer than in winter.

The time-latitude plots of the chlorophyll *a* concentrations (Fig. 6) illustrate the opposite phase between biomass in the region north of the frontal system and biomass within the frontal system. The most western panels (20 and 25E) are located in the retroflection area and show clearly a seasonal *W* shape (Fig. 6). Eastwards (30 to 45E), the southwest Indian background area (25–45E, 25–35S area defined in Table 2) exhibits also a *W* shape (Fig. 6).

5. Discussion

We demonstrated the seasonality in chlorophyll *a* mesoscale distribution in the Agulhas Current system. Time-longitude and time-latitude diagrams of chlorophyll *a* concentrations corroborate results from the power Hovmöller analysis: within the double frontal system formed by the AF and STF there is an extended temporal chlorophyll *a* maximum in spring-summer-fall and a well-marked minimum in winter, in phase opposition with the region north of the frontal system. Our results may help to resolve differences in prior efforts to estimate the seasonality of the Agulhas Current system, and to provide dynamical scenarios in agreement with the spatial-temporal distribution of chlorophyll pigment concentration in the area.

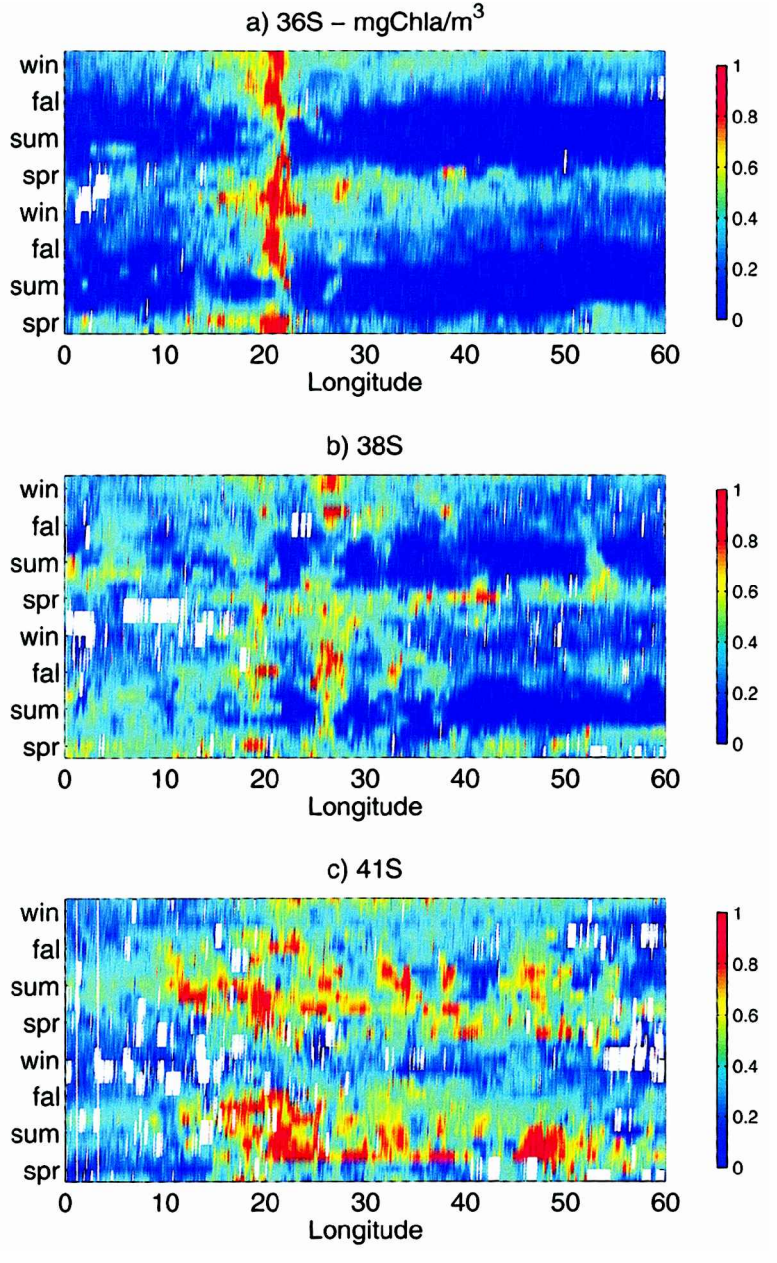

Figure 5. Time-longitude diagram of SeaWiFS chlorophyll concentrations (mgChl*a*/m^3) at (a) 36S, (b) 38S and (c) 41S, for two years of SeaWiFS data (October 1997–September 1999).

a. Seasonality of the AC volume

Modeling studies (Lutjeharms and van Ballegooyen, 1984; De Ruijter and Boudra, 1985; Ou and De Ruijter, 1986) suggested that the Agulhas Current (proper) volume is

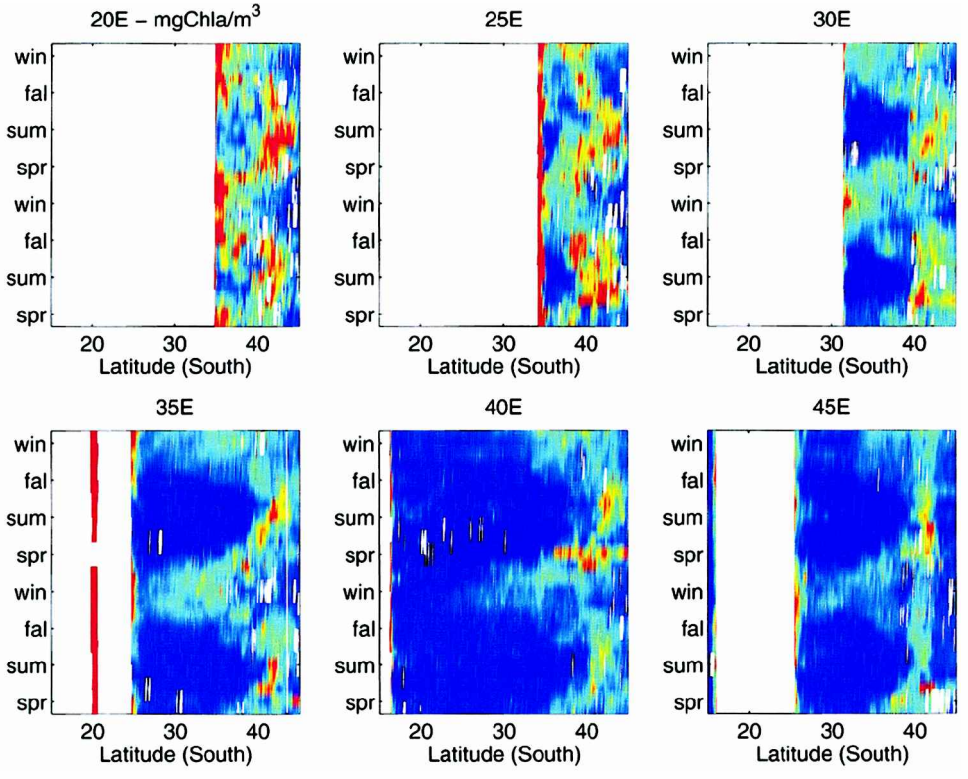

Figure 6. Time-latitude diagram of SeaWiFS chlorophyll concentrations (mgChl*a*/m^3) at 20E, 25E, 30E, 35E, 40E, 45E, for two years of SeaWiFS data (October 1997–September 1999). Color bar is as in Figure 5.

decisive in causing either westward penetration or upstream retroflection, a more southward penetration of the AC and greater intensity of the ARC. A high AC transport would initiate upstream retroflection of the AC resulting in the development of a well defined and pronounced Rossby wave. The seasonal oscillation of the sea-surface height variability, as deduced from satellite altimeter data, is characterized by a maximum (minimum) in austral summer (winter) (Quartly and Srokosz, 1993; Matano *et al.,* 1998). The summer maximum anomaly is associated with a southward extension of the high variability area (Matano *et al.,* 1998). The inshore portion of the AC might still flow as far west as 18E while the offshore portion of the current is inertially forced to leave the coast sooner (upstream retroflection), thereafter becoming trapped by the Agulhas Plateau. In conflict with this seasonal picture, calculations based on *in situ* hydrographic data showed there were no significant seasonal variations in the mean flow intensity of the upstream Agulhas Current (Pearce and Gründlingh, 1982; Ffield *et al.,* 1997). Matano *et al.* (1999) recently concluded that seasonal variations in the Agulhas retroflection region are not related to changes in the

upstream transport of the AC, which are regarded as negligible, but to local interactions of the current with the wind forcing and bottom topography. Biastoch *et al.* (1999) showed that the contribution of Tropical Surface Waters (TSW) to AC waters, via the Mozambique Channel, has an influence on the AC volume variability. The AC, fed by its sources, then presents its highest (lowest) southward transport during the October and November (March–April) months, in disagreement with some previous studies.

Whether the AC transport is higher during summer or winter is still unclear from both observations and modeling. Nevertheless, our results seem to support Matano *et al.*'s (1998) hypothesis: the seasonal differences in sea-surface height variability result from the displacements of the AC mean path. At 36S the AC leaves the continental shelf and flows along the Agulhas Bank. Depending on the strength of the AC transport, the AC will flow more or less offshore. The chlorophyll *a* time-longitude diagram across the AC at 36S (Fig. 5a) exhibits a clear seasonal cycle with patches of high chlorophyll concentrations around 20–23E when the AC meets the Agulhas Bank. In summer, these patches present a restricted longitudinal extent suggesting an upstream retroflection and a seasonally varying AC path in this region.

b. Dynamical scenarios and cross-frontal transport

We provide a schematic in Figure 7 to interpret our results. The surface waters in the frontal system, consisting of the area between the ARC and STC, is a mixing of Agulhas Water (AW), Subtropical Surface Water (STSW) of Atlantic and Indian origins, and Subantarctic Surface Water (SASW) (Fig. 7) (Gordon *et al.,* 1987; Read and Pollard, 1993). Southward of the STC, SASW is the predominant water mass. Northward of the frontal system, a mixture of STSW and Tropical Surface Water (TSW) is present (Fig. 6, Read and Pollard, 1993). The temperature, salinity characteristics of these water masses are summarized in Table 3. Modulation of the position of the high pressure system over the South Indian Ocean allows penetration of TSW in winter north of Madagascar in the Mozambique Channel (Fig. 7a) (Biastoch *et al.,* 1999) favoring intensification of cross-frontal mixing. Indeed mixing of TSW and STSW in winter north of the frontal system increases the thermal gradient across the AF in comparison with summer months, when no signature of TSW is expected (Fig. 7a,b) (Biastoch *et al.,* 1999). This is shown in Figure 3 where both winter and fall periods present higher average variance for SST at the AF (between 37 and 38S). Weeks and Shillington (1996), examining ocean color and SST data from early 1982 (January, February, March composites) and early 1983, pointed out a pronounced interannuality. In the chlorophyll composite, they related to 1982 a broad diffuse biological front compared with 1983 which presents a well-defined wave for the AF. Stronger SST gradients were calculated for 1982. When thermal surface gradients are stronger, cross-frontal transport is enhanced, supplying nutrients to sustain phytoplankton growth. Weeks *et al.* (1998), analyzing a three-year period of multichannel SST data, found the winter SST gradients considerably stronger than those in summer strengthening our analysis of the surface water masses (Fig. 7). The ARC skirted the northern edge of the

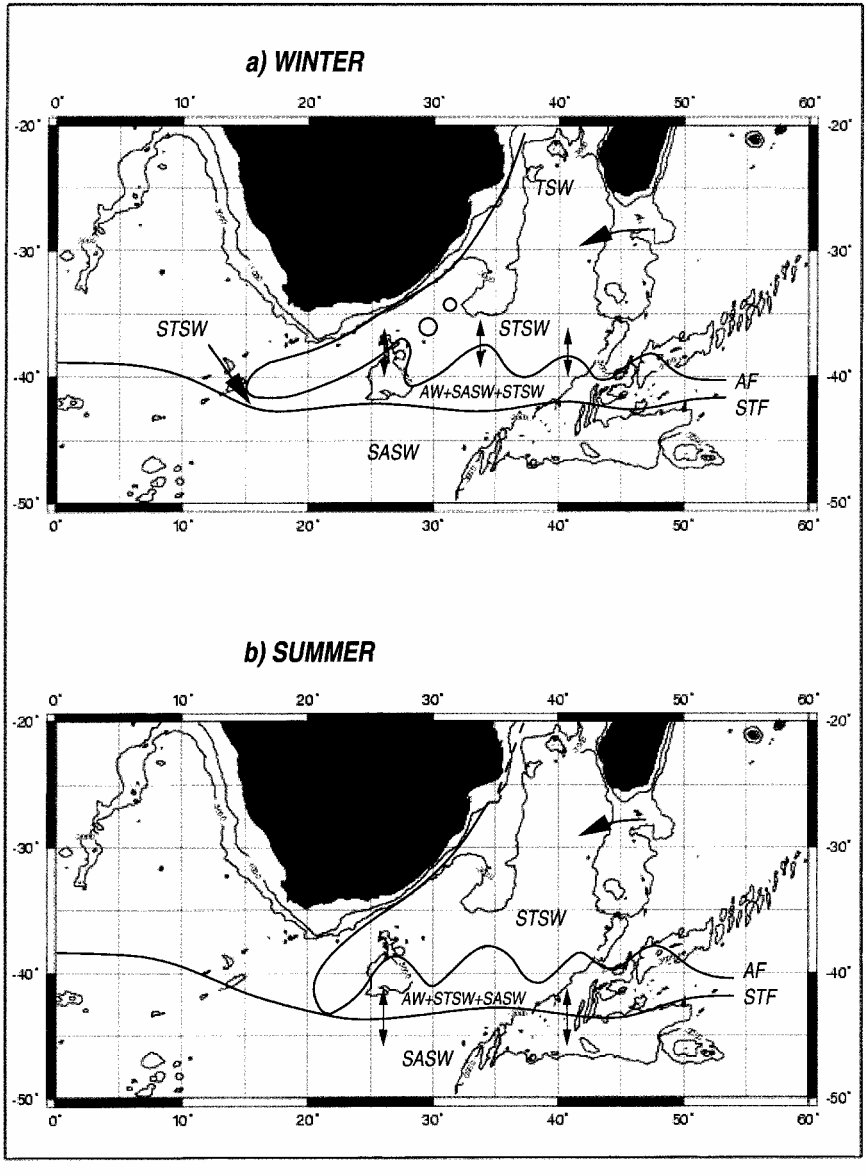

Figure 7. Scheme of the dynamical scenarios established for austral (a) winter and (b) summer conditions. Vertical double arrows denote enhanced cross frontal mixing.

Agulhas Plateau in winter, and, in contrast, the strongest gradients appeared on the southern boundary of the Agulhas Plateau (AP) in summer (Fig. 7). Stronger gradients in winter are favorable to induce a more diffuse chlorophyll *a* signature of the ARC wave.

Moreover, due to a less southward penetration of the AC in winter, Atlantic STSW,

Table 3. Characteristics of surface water masses (Temperature (°C) and Salinity (psu)). Values are deduced from Gordon and Molinelli (1982), Gordon *et al.* (1987), Read and Pollard (1993) and Holliday and Read (1998).

	Temperature (°C)	Salinity (psu)
Tropical Surface Water (TSW)	>23	<35.4
Agulhas Water (AW)	14–17	35.2–35.35
Indian	15–24	35.4–35.6
Subtropical Surface Water (STSW)		
Atlantic	16–22	35.2–35.5
Subantarctic Surface Water (SASW)	3–8	33.8–34.7

fresher than the Indian STSW (Table 3), could intrude in a larger amount between the fronts and a higher salinity gradient across the AF may also result. The South Atlantic water would enter the Agulhas retroflection from the south, swept into the retroflection region to the east of each of the Agulhas rings, and not from AC flow through the Agulhas Passage (Gordon *et al.,* 1987).

In addition to cross-frontal transport, the zonal movement of the zero wind stress curl linked to the movement of the high pressure system could also contribute to the chlorophyll *a* seasonality in the background of the southwest Indian Ocean. Indeed, August presents a strengthening of the wind stress over the subtropical gyre (north of 45S) (Matano *et al.,* 1999, Fig. 9). Hence, nutrients could be supplied in the upper ocean by deepening of the mixed-layer depth enabling an increase in new production and phytoplankton stock.

c. Effect of frontal dynamics on biological response

Highest chlorophyll *a* concentrations of the Agulhas system were found between the AF and the STF in spring and summer. The wavelet analysis informed us about the location of the biological enrichment in relation to the dynamical fronts (given by the power Hovmöller of the SLA). However, the causes of the confinement of high chlorophyll *a* levels between the fronts are still not well understood. In winter, significant deepening of the mixed layer due to strong wind events and light limitation constitute two factors likely to limit phytoplankton growth and thus induce low chlorophyll *a* levels within the frontal system.

Spall and Richards (2000), studying mesoscale frontal instabilities and plankton dynamics, investigated contrasting physical frontal set-ups and their impact on the ecosystem reaction. They showed that the gradient in isopycnal layer thickness across a jet plays a large role in the dynamics of producing cross-frontal transports. A large gradient in isopycnic layer thickness allows a very dynamic change in relative vorticity, compared to a more symmetric jet evolution when gradients in isopycnic layer thickness are less. In the former case, cross-frontal transport is important with vertical fluxes of tracers as a result of flow along sloping isopycnals. In the latter, water following the jet is unable to escape and forms a barrier to mixing across the jet axis. In our region, the situation is complicated by the presence of a double front: the AF with a strong thickness variation in certain isopycnic

layers and a large slope in the isopycnals below the mixed layer, and the STF exhibiting a less pronounced slope of isopycnals and a moderate gradient in isopycnic layer thickness (see for a typical summer situation Figure 4 in Read and Pollard, (1993)). In winter, information on the density vertical structure is still scarce. The ecosystem response is most likely driven by the juxtaposition of both fronts and the seasonal changes in their density strength.

A greater understanding of the respective roles of physical and biogeochemical processes in setting and modulating the chlorophyll *a* distribution variability can only be achieved through both modeling and *in situ* joint physical/biological studies in the Agulhas system to test the scenarios put forward.

Acknowledgments. Support for this work was provided by a grant from the Centre National de la Recherche Scientifique (SeaWiFS-France) to LEGOS. Ocean color data used in this study were produced by the SeaWiFS Project at Goddard Space Flight Center. Data were obtained from the Goddard Active Archive Center under the auspices of the National Aeronautics and Space Administration. SST products were obtained from The Naval Oceanographic Office through Bruce McKenzie's help. Wavelet software was provided by C. Torrence and G. Compo and is available at URL://paos.colorado.edu/research/wavelets/. We thank J. Lutjeharms and F. Shillington for fruitful discussions during E.M.'s stay at University of Cape Town. We wish to also thank Y. H. Park and I. Dadou for their helpful comments and three anonymous reviewers for their constructive critical reading of the manuscript.

REFERENCES

Belkin, I. M. and A. L. Gordon. 1996. Southern Ocean fronts from the Greenwich meridian to Tasmania. J. Geophys. Res., *101,* 3675–3696.

Biastoch, A., C. J. C. Reason, J. R. E. Lutjeharms and O. Boebel. 1999. The importance of flow in the Mozambique Channel to seasonality in the greater Agulhas Current system. Geophys. Res. Lett., *26,* 3321–3324.

De Ruijter, W. P. M. and D. B. Boudra. 1985. The wind driven circulation in the South Atlantic–Indian Ocean—I. Numerical experiments in a one layer model. Deep-Sea Res., *32,* 557–574.

Ducet, N., P. Y. Le Traon and G. Reverdin. 2000. Global high resolution of ocean circulation from TOPEX/POSEIDON and ERS-1/2. J. Geophys. Res., *105*(C8), 19477–19498.

Farge, M. 1992. Wavelet transform and their application to turbulence. Ann. Rev. Fluid Mech., *24,* 395–457.

Feron, R. C. V., W. P. M. De Ruijter and P. J. van Leeuwen. 1998. New method to determine the mean ocean circulation from satellite altimetry. J. Geophys. Res., *103,* 1343–1362.

Ffield, A., J. Toole and D. Wilson. 1997. Seasonal circulation in the South Indian Ocean. Geophys. Res. Lett., *24,* 2773–2776.

Flierl, G. R. and C. Davies. 1993. Biological effects of Gulf Stream meandering. J. Mar. Res., *51,* 529–560.

Gordon, A. L. 1986. Inter-ocean exchange of thermocline water. J. Geophys. Res., *91,* 5037–5046.

Gordon, A. L., J. R. E. Lutjeharms and M. L. Gründlingh. 1987. Stratification and circulation at the Agulhas Retroflection. Deep-Sea Res., *34,* 565–599.

Gordon, A. L. and E. Molinelli. 1982. Southern Ocean Atlas, Columbia University Press, NY, 274 pp.

Gordon, A. L., R. F. Ukiss, W. M. Smethie and M. J. Warner. 1992. Thermocline and intermediate

water communication between the South Atlantic and Indian Ocean. J. Geophys. Res., *97,* 7223–7240.

Holliday, N. P. and J. F. Read. 1998. Surface oceanic fronts between Africa and Antarctica. Deep-Sea Res., *45,* 217–238.

Le Traon, P. Y., F. Nadal and N. Ducet. 1998. An improved mapping method of multisatellite data. J. Atmos. Oceanic Tech., *13,* 522–534.

Lutjeharms, J. R. E. 1988. On the role of the East Madagascar Current as a source of the Agulhas Current. S. Afr. J. Sci., *84,* 236–238.

Lutjeharms, J. R. E. and E. Machu. 2000. On kinematic upwelling inshore of the East Madagascar current. Deep-Sea Res., *47,* 2341–2369.

Lutjeharms, J. R. E. and H. R. Valentine. 1984. Southern Ocean thermal fronts south of Africa. Deep-Sea Res., *31,* 1461–1475.

Lutjeharms, J. R. E. and R. C. van Ballegooyen. 1984. Topographic control in the Agulhas Current system. Deep-Sea Res., *11,* 1321–1337.

Machu, E., B. Ferret and V. Garçon. 1999. Phytoplankton pigment distribution from SeaWiFS data in the subtropical convergence zone south of Africa: a wavelet analysis. Geophys. Res. Lett., *26,* 1469–1472.

Matano, R. P., C. G. Simionato, W. P. De Ruijter, P. J. van Leeuwen, P. T. Strub, D. B. Chelton and M. G. Schlax. 1998. Seasonal variability in the Agulhas Retroflection region. Geophys. Res. Lett., *25,* 4361–4364.

Matano, R. P., C. G. Simionato and P. T. Strub. 1999. Modelling the wind-driven variability of the South Indian Ocean. J. Phys. Oceanogr., *29,* 217–230.

May, D. A., M. M. Parmeter, D. S. Olszewski and B. D. McKenzie. 1998. Operational processing of satellite sea surface temperature retrievals at the Naval Oceanographic Office. Bull. Amer. Met. Soc., *79*(3), 397–407.

McClain, C. R., M. L. Cleave, G. C. Feldman, W. W. Gregg, S. B. Hooker and N. Kuring. 1998. Science quality SeaWiFS data for global biosphere research. Sea Tech., *39,* 10–16.

McGillicuddy, D. J. Jr., A. R. Robinson, D. A. Siegel, H. W. Jannasch, R. Johnson, T. D. Dickey, J. McNeil, A. F. Michaels, and A. H. Knap. 1998. Influence of mesoscale eddies on new production in the Sargasso Sea. Nature, *394,* 263–266.

Oschlies, A. and V. C. Garçon. 1998. Eddy-induced enhancement of primary production in a model of the North Atlantic Ocean. Nature, *394,* 266–269.

Ou, H. W. and W. P. M. De Ruijter. 1986. Separation of an inertial boundary current from a curved coast line. J. Phys. Oceanogr., *16,* 280–289.

Pearce, A. F. and M. L. Gründlingh. 1982. Is there a seasonal variation in the Agulhas Current? J. Mar. Res., *40,* 177–184.

Quartly, G. D. and M. A. Srokosz. 1993. Seasonal variations in the region of the Agulhas retroflection: studies with Geosat and FRAM. J. Phys. Oceanogr., *23,* 2107–2124.

Read, J. F. and R. T. Pollard. 1993. Structure and transport of the Antarctic circumpolar current and Agulhas return current at 40E. J. Geophys. Res., *98,* 12281–12295.

Spall, S. A. and K. J. Richards. 2000. A numerical model of mesoscale frontal instabilities and plankton dynamics. I. Model formulation and initial experiments. Deep-Sea Res. I, *47,* 1261–1301.

Stramma, L. and J. R. E. Lutjeharms. 1997. The flow field of the subtropical gyre in South Indian Ocean. J. Geophys. Res., *102,* 5513–5530.

Torrence, C. and G. P. Compo. 1998. A practical guide to wavelet analysis. Bull. Amer. Met. Soc., *79*(1), 61–78.

Weeks, S. J. and F. A. Shillington. 1994. Interannual scales of variation of pigment concentrations

from coastal zone colour scanner data in the Benguela upwelling system and the subtropical convergence zone south of Africa. J. Geophys. Res., *99,* 7385–7399.

—— 1996. Phytoplankton pigment distribution and frontal structure in the subtropical convergence region south of Africa. Deep-Sea Res., *43,* 739–768.

Weeks, S. J., F. A. Shillington and G. B. Brundrit. 1998. Seasonal and spatial SST variability in the Agulhas retroflection and Agulhas return current. Deep-Sea Res., *45,* 1611–1625.

Received: *10 April, 2000;* revised: *2 August 2001.*